Nuclear Instruments and Methods in Physics Research A 1080 (2025) 170721

Contents lists available at ScienceDirect

Nuclear Inst. and Methods in Physics Research, A

journal homepage: www.elsevier.com/locate/nima

Development and validation of gamma-ray dose measurement method using glass dosimeter covered with mixed material filters in a high-energy gamma-ray field

K. Aoki, Z. Xu, M. Matsuki, S. Kusaka, S. Tamaki, F. Sato, I. Murata *

Graduate School of Engineering, The University of Osaka, Yamada-oka 2-1, Suita, Osaka, 565-0871, Japan

ARTICLE INFO

Keywords:
Boron neutron capture therapy (BNCT)
RPLGD
Bayesian estimation
Air kerma
Mixed radiation field
Dose estimation

ABSTRACT

Boron Neutron Capture Therapy (BNCT) is a next-generation radiation therapy that utilizes the nuclear reaction between neutrons and boron-10 (^{10}B) to selectively destroy cancer cells. In the treatment field of BNCT, secondary gamma rays are generated from neutron capture reactions, resulting in forming of a mixed field of neutrons and gamma rays. Therefore, in order to accurately determine the patient's exposure dose, it is necessary to separately measure neutron and gamma-ray doses. To address this, our research group has proposed and been investigating the "Shielding Filter Method", which estimates gamma-ray doses by using two radiophotoluminescence glass dosimeters (RPLGD), adjusting the sensitivity by covering each dosimeter with an appropriate shielding filter, and making the difference between the measured results. In the previous study, we first aimed to measure gamma-ray doses using a single filter in a gamma-only field. As a result, it was found that the measured dose had a large error when the incident angle of the gamma-rays to the glass dosimeter was large. In this study, we optimized the design by thinning the filter and adjusting the placement of filter materials, and by adding filter covers in both ends. Consequently, the reproducibility of the air kerma coefficient within a 6.1 % error was confirmed for the entire energy range up to 10 MeV. Furthermore, irradiation experiments using gamma-ray standard sources were conducted and the obtained results were consistent with both the PHITS simulation results and theoretical values within an acceptable error. Going forward, we plan to design and manufacture two types of filters for two glasses to verify whether gamma-ray doses can be measured in a mixed neutron and gamma-ray field.

1. Introduction

1.1. Boron Neutron Capture Therapy

In recent years, Boron Neutron Capture Therapy (BNCT) has gained attention as a new radiation therapy for cancer. In 2020, BNCT was approved for insurance coverage in Japan for the treatment of unresectable locally advanced or locally recurrent head and neck cancer [1]. BNCT is a treatment that selectively kills cancer cells by utilizing the nuclear reaction between boron and neutrons. First, a high concentration of a^{10}B-based drug is accumulated in the cancer cells. Then, neutrons are irradiated, and the cancer cells are destroyed by alpha particles (^{4}He) and lithium (^{7}Li) nuclei produced by the nuclear reaction of ^{10}B(n, α)^{7}Li. This reaction is represented by the following equation.

$$\begin{aligned} n + {}^{10}B &\rightarrow {}^{4}He + {}^{7}Li + 2.79\ \text{MeV}\ (6\%) \\ &\rightarrow {}^{4}He + {}^{7}Li^{*} + 2.31\ \text{MeV}\ (94\%) \\ {}^{7}Li^{*} &\rightarrow {}^{7}Li + \gamma\ (478\ \text{keV}) \end{aligned} \quad (1)$$

The alpha particles and ^{7}Li nuclei produced in this reaction have an extremely short range (approximately 4–9 μm), which allows the selective destruction of cancer cells that have taken up ^{10}B without affecting the surrounding healthy cells [2]. Various fields of research are being widely pursued to promote the spread of BNCT. One of the most important challenges in this area is the development of a high-intensity neutron source, as BNCT requires a thermal or epithermal neutron source with a flux of about 1×10^{9}n/sec/cm^{2}. Until 2019, BNCT was only conducted using research nuclear reactors. Recently, accelerator-based neutron sources (ABNS) have been developed as alternatives to reactors for the use in BNCT.

* Corresponding author.
E-mail address: murata@see.eng.osaka-u.ac.jp (I. Murata).

https://doi.org/10.1016/j.nima.2025.170721
Received 9 November 2024; Received in revised form 29 April 2025; Accepted 1 June 2025
Available online 6 June 2025

1.2. Objectives

In radiation therapies, dose measurement for both patients and radiation workers are of utmost importance. In BNCT using ABNS, high-energy secondary gamma-rays of up to 10 MeV are generated due to neutron capture reactions between thermal neutrons and surrounding various materials, resulting in a mixed field of neutrons and high-energy gamma-rays. Therefore, it is essential to accurately measure the gamma-ray dose generated simultaneously with neutrons. However, most dosimeters are sensitive to both neutrons and gamma-rays, making it difficult to separate them and measure their doses.

To date, several methods have been proposed for measuring gamma-rays in the mixed field, including thermoluminescence dosimeters (TLD) [3,4] and twin ionization chambers [5,6]. However, each method has its own limitations. TLDs suffer from issues like fading, which leads to information loss, and they cannot be read repeatedly. The twin ionization chamber has poor spatial resolution because its detector is so large that it distorts the neutron and gamma-ray field. Various other detectors have also been explored [7–9] but measuring in the mixed field remains a challenging and time-consuming task.

In Osaka University's BNCT project, RPLGD (Radiophotoluminescence Glass Dosimter) has been adopted as the dosimeter used in the irradiation filed [10–12]. RPLGDs are made from melted glass, which contributes to improved reproducibility and consistency in dose reading compared to TLDs. RPLGDs also exhibit low energy dependence of approximately 20 %, irrespective of the constituent material, and demonstrate a fading effect of less than 5 % per year due to the stability of radiation-induced fluorescence centers. Additionally, they are smaller than twin ionization chambers, providing better spatial resolution. However, since RPLGDs are sensitive to both neutrons and gamma rays, it was impossible to separately measure gamma-ray and neutron doses in the mixed field [13].

To address this issue, our group developed the "lead filter method" [14], which used lead filters to estimate gamma-ray doses measured by RPLGDs. This method takes advantage of the fact that neutrons can pass through an appropriately thick lead shield while gamma rays are partially blocked. However, this method was ineffective for gamma-rays with energies above 1 MeV. Therefore, Tochitani improved the design of the lead filter that covers the glass dosimeter, demonstrating that, when the gamma-rays spectrum is known, the energy dependence can be controlled up to 10 MeV [15]. Nonetheless, their method required prior knowledge of the gamma-ray energy spectrum, and the process of determining the optimal filter design was not standardized, relying on trial and error. To overcome these challenges, Kamisaki proposed a method for accurately measuring gamma-ray doses using shielding filters with several kinds of material, even when the gamma-ray energy spectrum is unknown. Their results showed that the air dose in a gamma-ray only field could be accurately measured regardless of the incident photon's energy spectrum [16]. However, the thicknesses of the filters were not fixed to be a constant value and thick, e.g., with a maximum thickness of 10 mm. The study finally highlighted the need for thinner filters to reduce the effects of incident angle on the glass dosimeter.

In this study, we aim to reduce the impact of the incident angle to the glass by making the filter thickness uniform and thinner. We also optimized the filter arrangement and fabricated a filter with a cover. The filter was tested through gamma-ray irradiation experiments from various angles, leading to the successful completion of the final filter design.

2. Materials and methods

2.1. Radiophoto-luminescence glass dosimeter (RPLGD)

The radiophotoluminescence glass dosimeter (RPLGD) is an integrating-type solid-state dosimeter ([13]; ATGC, 2014). By using silver-activated phosphate glass as the material, after irradiating an RPLGD with ionizing radiation, the RPLGD emits orange fluorescence by ultraviolet light excitation. This phenomenon is called radiophotoluminescence (RPL), and it is known that the amount of fluorescence is proportional to the absorbed dose.

In this study, we used the GD-301 as the RPLGD and the Dose Ace FGD-1000 as the readout device [17]. Fig. 1 shows a photograph of the RPLGD we used. The GD-301 is a cylindrical element with a diameter of 1.5 mm and a length of 8.5 mm, with a readout area of 1.0 mm in diameter and 6.0 mm in length. Its composition by weight is 31.55 % P, 51.16 % O, 6.12 % Al, 11.00 % Na, and 0.17 % Ag, with a density of 2.61 g/cm^3 and an effective atomic number of 12.039. To read the dose measured by the GD-301, the FGD-1000 is equipped with a Laser Diode (LD)-pumped UV solid-state laser (Explorer 349, Spectra-Physics) [18]. LD refers to a semiconductor laser, which is a device that emits laser light by passing an electric current through a semiconductor. It is characterized by its high coherence, as it produces light with identical properties such as wavelength and phase. For further details on the laser, please refer to [19].

2.2. Shielding filter

2.2.1. Principle

In this study, we propose a shielding filter method for accurately measuring gamma-ray air dose by manipulating the response of the RPLGD to gamma rays using various filter materials for shielding. By adjusting the gamma-ray response to be proportional to the air kerma coefficient $\boldsymbol{\alpha}\left[\mu Gy/h/\left(cm^{-2}\,sec^{-1}\right)\right]$, this method allows for precise gamma-ray dose measurement. The definition of the filter and gamma-ray flux for the shielding filter method in a gamma-ray field is shown in Fig. 2. Here, the gamma-ray flux before passing through the filter is denoted as $\boldsymbol{\phi}_\gamma\left[cm^{-2}\,sec^{-1}\right]$ and the gamma-ray flux after passing through the filter is denoted as $\boldsymbol{\phi}_{\gamma A}\left[cm^{-2}\,sec^{-1}\right]$. Note that $\boldsymbol{\alpha}$, $\boldsymbol{\phi}_\gamma$ and $\boldsymbol{\phi}_{\gamma A}$ are energy dependent as $\alpha(E)$, $\phi_\gamma(E)$, $\phi_{\gamma A}(E)$, but are omitted here for simplicity.

The true gamma-ray air dose rate $D_\gamma[\mu Gy/h]$ is expressed using the air kerma coefficient $\boldsymbol{\alpha}$ in equation (2).

$$D_\gamma = \int \boldsymbol{\phi}_\gamma \boldsymbol{\alpha} dE \tag{2}$$

Next, the gamma dose $D_{\gamma A}[\mu Gy/h]$, measured by the dosimeter, is given by equation (3) using the response function $\boldsymbol{f}_A\left[\mu Gy/h/\left(cm^{-2}\,sec^{-1}\right)\right]$ for the gamma-ray flux $\boldsymbol{\phi}_\gamma$ before passing through the dosimeter filter. Similarly, the energy dependence is omitted for $\boldsymbol{f}_A$.

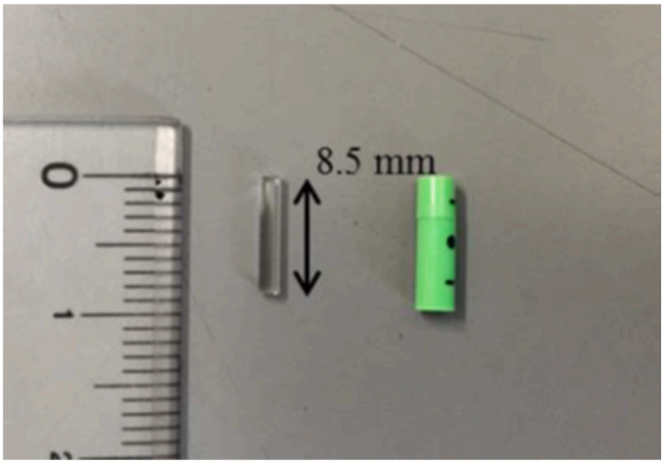

Fig. 1. Photo of RPLGD and its casing.

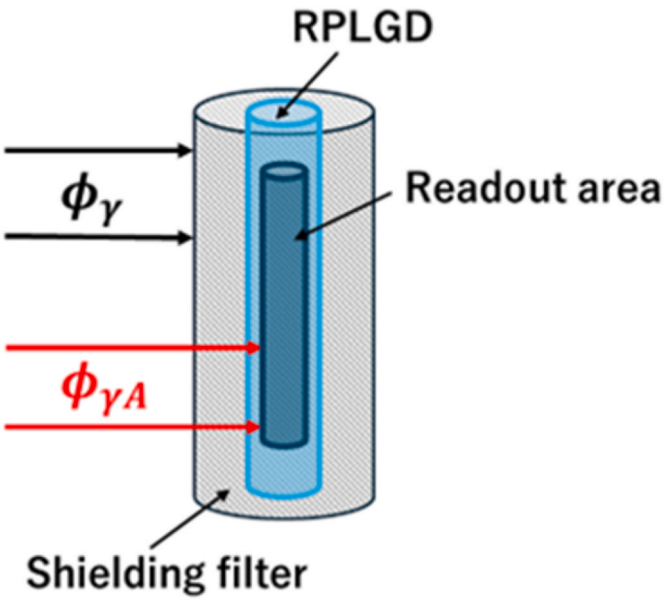

Fig. 2. Definition of filter and gamma flux for the shielding filter method in a gamma-ray field.

$$D_{\gamma A} = \int \boldsymbol{\phi}_\gamma \boldsymbol{f}_A dE \tag{3}$$

From equations (2) and (3), equation (4) is formally derived

$$D_\gamma = \frac{\int \boldsymbol{\phi}_\gamma \boldsymbol{\alpha} dE}{\int \boldsymbol{\phi}_\gamma \boldsymbol{f}_A dE} D_{\gamma A} = \eta D_{\gamma A} \tag{4}$$

As shown in equation (5), by designing the filter so that the response function $\boldsymbol{f}_A$ of the filter becomes a constant multiple of the air kerma coefficient $\boldsymbol{\alpha}$, η becomes constant. This allows for the calculation of the true gamma-ray air dose in a gamma-ray field with an unknown energy spectrum by applying the normalization factor η to the dosimeter's measured value.

$$\boldsymbol{\alpha} = \eta \boldsymbol{f}_A \tag{5}$$

We propose a method to achieve equation (5) by manipulating the response function $\boldsymbol{f}_A$ and to evaluate D_γ from $D_{\gamma A}$ by equation (4). Now, consider a dosimeter covered by filters made of multiple types of materials. As shown in equation (6), the response $\boldsymbol{f}_A$ can be expressed as the inner product of the response function matrix $\boldsymbol{R}$ and the material proportion ratio, that is, the height ratio vector $\boldsymbol{t}$. Here, the matrix component R_{ij} of the response function matrix $\boldsymbol{R}$ represents the absorbed dose rate per unit flux for i-th ($i = 1\sim$m) energy and j-th ($j = 1\sim$n) material.

$$\boldsymbol{f}_A = \begin{pmatrix} f_1 \\ \vdots \\ f_m \end{pmatrix} = \begin{pmatrix} R_{11} & \cdots & R_{1n} \\ \vdots & \ddots & \vdots \\ R_{m1} & \cdots & R_{mn} \end{pmatrix} \begin{pmatrix} t_1 \\ \vdots \\ t_n \end{pmatrix} = \boldsymbol{R} \cdot \boldsymbol{t} \tag{6}$$

where $\boldsymbol{t}$ satisfies $\sum \boldsymbol{t} = 1$. Therefore, by solving this matrix equation with respect to $\boldsymbol{t}$, we can theoretically design a filter that provides the dosimeter with an arbitrarily set response $\boldsymbol{f}_A$. In this study, Bayesian estimation was used to solve this matrix equation for $\boldsymbol{t}$. Details of the Bayesian estimation method described in the next section. The air kerma coefficient $\boldsymbol{\alpha}$ for each photon energy was taken from the values specified by ICRP74 [20], as shown in Fig. 3 and Table 1.

2.2.2. Bayesian estimation method

The Bayesian estimation method is based on Baye's theorem, which is known as conditional probability. Iwasaki developed the spectrum-type Bayesian estimation method, recognized as an extended interpretation of Bayes' theorem, as one of the solutions to the inverse problems in radiation measurement [21,22]. In this study, we applied the spectrum-type Bayesian estimation method to solve equation (5) and finally derive $\boldsymbol{t}$.

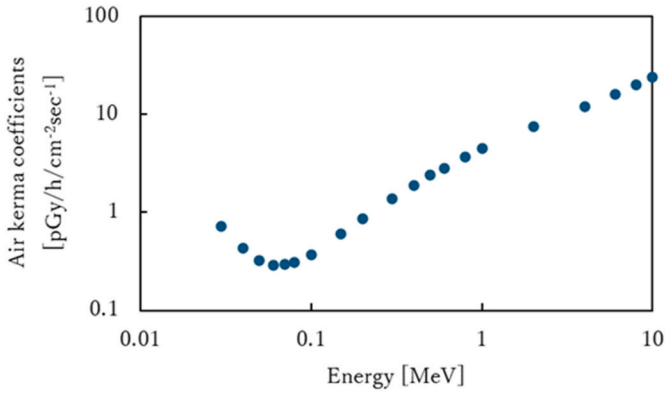

Fig. 3. Air kerma coefficients [20].

Table 1
Detailed values of the Air kerma coefficient [20].

Energy [MeV]	Air kerma coefficients [pGy/h/cm^{-2}sec^{-1}]	Energy [MeV]	Air kerma coefficients [pGy/h/cm^{-2}sec^{-1}]
0.03	0.721	0.4	1.89
0.04	0.429	0.5	2.38
0.05	0.323	0.6	2.84
0.06	0.289	0.8	3.69
0.07	0.298	1	4.47
0.08	0.307	2	7.55
0.1	0.371	4	12.1
0.15	0.599	6	16.1
0.2	0.856	8	20.1
0.3	1.38	10	24.0

In the spectrum-type Bayesian estimation, the obtained posterior probability (the estimated $\boldsymbol{t}$) is used again as the prior probability in the next iteration of the Bayesian estimation.

First, the response function matrix $\boldsymbol{R}$ in equation (6) is normalized as shown in equation (7), where f_j is defined as equation (8), which is the normalization factor.

$$R'_{ij} = \frac{R_{ij}}{f_j} \tag{7}$$

$$f_j = \sum_{i=1}^{m} R_{ij} \tag{8}$$

Here, equation (6) can be rewritten as equation (9) by using the normalization matrix $\boldsymbol{F}$ in equation (10).

$$\boldsymbol{\alpha} = \eta \boldsymbol{R}' \cdot \boldsymbol{F} \cdot \boldsymbol{t}, \tag{9}$$

$$\boldsymbol{F} = \begin{pmatrix} f_1 & & \varnothing \\ & \ddots & \\ \varnothing & & f_n \end{pmatrix} \tag{10}$$

where, $\boldsymbol{\alpha}$ is provided in Fig. 3, $\boldsymbol{R}'$ (and $\boldsymbol{R}$) are determined through numerical calculations presented in the following section, and $\boldsymbol{F}$ is derived from $\boldsymbol{R}$. By solving equation (10), $\boldsymbol{t}$ can be determined, and since $\sum \boldsymbol{t} = 1$, η can also be fixed. Then, the estimated effective height ratio is defined as $\boldsymbol{est} = \eta \boldsymbol{F} \boldsymbol{t}$, and the following equation becomes the one which we should solve.

$$\boldsymbol{\alpha} = \boldsymbol{R}' \cdot \boldsymbol{est} \tag{11}$$

To iteratively apply the Bayesian estimation method, we introduce the estimated height ratio $est_j^{(k)}$, where the superscript (k) indicates the k-th iteration. According to Iwasaki, when the condition α_i is given, $est_j^{(k+1)}$ can be expressed as follows using $est_j^{(k)}$.

$$est_j^{(k+1)}(i) = \alpha_i \frac{R'_{ij} est_j^{(k)}}{\sum_{j=1}^{n} R'_{ij} est_j^{(k)}}, \tag{12}$$

where $est_j^{(k)}$ corresponds to the prior probability, and $est_j^{(k+1)}$ corresponds to the posterior probability. The subscript i means revision by α_i value. Summing all components α_i of $\boldsymbol{\alpha}$, the finally equation is expressed as follows.

$$est_j^{(k+1)}(i) = \sum_{i=1}^{m} \alpha'_i \frac{R'_{ij} est_j^{(k)}}{\sum_{j=1}^{n} R'_{ij} est_j^{(k)}} \tag{13}$$

This equation forms the fundamental expression of the spectrum-type Bayesian estimation. Consequently, after k iterations of the Bayesian estimation, the height ratio $\boldsymbol{t}$ is obtained from $est_j^{(k+1)}$ as follows.

$$\eta \boldsymbol{t} = \boldsymbol{F}^{-1} \cdot \boldsymbol{est}^{(k+1)} \tag{14}$$

The material height ratio $\boldsymbol{t}$ must be normalized using $\sum_i t_i = 1$, and the normalization factor η is finally obtained by summing both sides of equation (14) as in the next equation.

$$\eta = \sum \left(\boldsymbol{F}^{-1} \cdot \boldsymbol{est}^{(k)} \right) \tag{15}$$

2.3. Simulation

In this study, the $\boldsymbol{R}$ matrix from equation (6) was evaluated through simulations. For the simulations, the Particle and Heavy Ion transport code System (PHITS), developed by the Japan Atomic Energy Agency, the Center for Computational Science, and the High Energy Accelerator Research Organization, was used [23]. PHITS, which integrates EGS5 implementing a mode capable of accurately calculating the electromagnetic cascade including interactions between photons, X-rays, and electrons, was adopted to precisely evaluate the absorbed dose.

In the simulation, filters of various thickness were irradiated with monoenergetic gamma rays monoenergetic gamma rays to determine the response of the RPLGD. A monoenergetic point gamma-ray source was employed, and 20 energy bins between 0.03 and 10 MeV were selected, as shown in Table 1. Based on this, 20 different monoenergetic gamma rays were simulated. The filter was placed only outside the reading area of the RPLGD as illustrated in Fig. 4. The absorbed dose in the reading region was tallied using the [T-Deposit] of PHITS. The distance between the source and the RPLGD was set to 5 cm, ensuring the maximum incident angle of the gamma-rays was within 5 deg.

The absorbed dose calculated by [T-Deposit] is expressed in units of [Gy/source], and to match the units with the air kerma coefficient, the values were converted to $[\mu\ \mathrm{Gy/h}/(cm^{-2}\ sec^{-1})]$. For evaluating the performance of the filter in this study, the mean absolute percentage error (MAPE), ε, defined as in equation (16) was introduced to assess the error with equal precision in all the energy bins. Here, A_i and $\widehat{A_i}$ represent the i-th elements of the target value vector and the measured value vector, respectively. In this study, the target value vector A was set as the air kerma coefficient $\boldsymbol{\alpha}$, and the measured value vector $\widehat{\boldsymbol{A}}$ was the adjusted filter response $\eta \boldsymbol{f}_A$ defined in Equation (5).

$$\varepsilon = \frac{1}{m} \sum_{i=1}^{m} \left| \frac{\widehat{A_i} - A_i}{A_i} \right| \tag{16}$$

Next, the effect of the irradiation angle was investigated. It is known that the shielding material filter method is influenced by the incident angle of irradiated gamma-ray. Therefore, simulations were conducted for different irradiation angles on the glass dosimeter, and the impact of the irradiation angle was verified. Fig. 5 illustrates the simulation model in PHITS to examine the effect of irradiation angles. The gamma-ray source condition was the same as in Fig. 4, and nine irradiation angles from −60 deg to 60 deg in 15 deg increments were used. The index used to evaluate the influence of irradiation angle was the mean percentage error in equation (17).

$$\varepsilon = \frac{1}{m} \sum_{i=1}^{m} \frac{\widehat{A_i} - A_i}{A_i} \tag{17}$$

3. Shielding filter design and irradiation experiments

3.1. Shielding filter design

3.1.1. Filter material selection

In this study, we examined whether accurate dose measurement could be achieved by wrapping a shielding filter around a single RPLGD in a gamma-only field to control the response. Here, we present the results regarding the selection of materials for the filter design. For the design of the filter we solved equation (6) to obtain $\boldsymbol{t}$. First, we fixed filter thickness to be 1.0 mm and created the response function matrix $\boldsymbol{R}$ for 13 materials as shown in Table 2. Subsequently, we estimated $\boldsymbol{t}$ using the spectrum-type Bayesian estimation method. The results of the filter design are shown in Fig. 6 and Table 2.

Next, we arranged the filter materials in order of carbon (C), nickel (Ni) and tungsten (W) from the bottom, as shown in Fig. 6, and conducted irradiation simulation calculations using PHITS with gamma-ray irradiation angles ranging from −60 deg to 60 deg. The results are

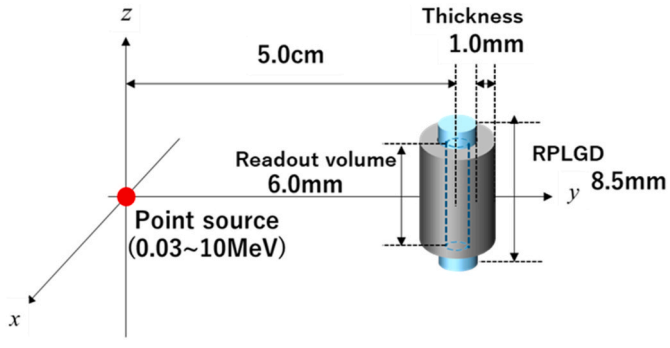

Fig. 4. Simulation model for evaluating the response function matrix $\boldsymbol{R}$ by PHITS.

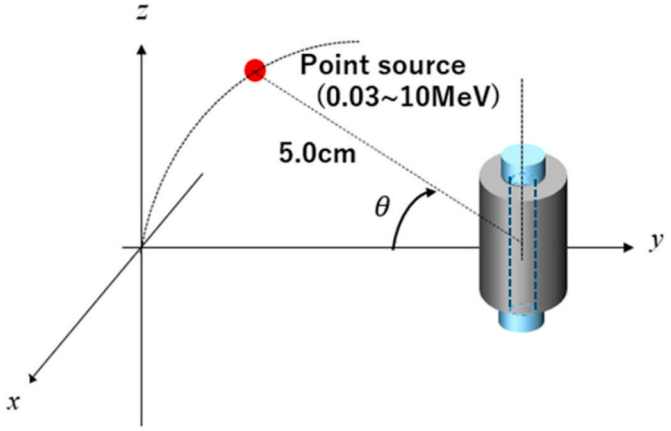

Fig. 5. Simulation system for examining the effects of irradiation angle.

Table 2
Results of filter height ratio.

Material	Height ratio
Al	0
Bi	0
C	0.2178
Fe	0
HDPE	0
Nb	0
Ni	0.4954
POM	0
PTFE	0
Sn	0
V	0
W	0.2868
Zn	0

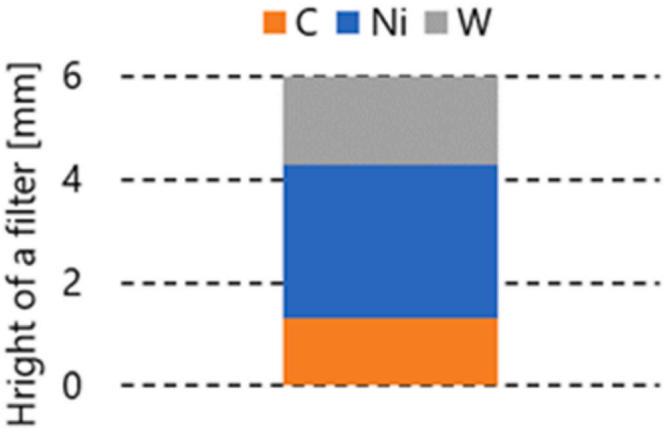

Fig. 6. Filter design results.

presented in Fig. 7. Based on the simulations system in Fig. 5, the irradiation distance and gamma-ray energy are the same as the conditions shown in Section 2.3. The results show the average percentage error relative to 0 deg.

From Fig. 7, it can be observed that when the irradiations angle is negative, the response is greater compared to 0 deg, while for positive angles, the response is smaller, This is attributed to the fact that for negative angles, gamma-ray enter from the side of carbon (C), resulting in a higher proportion of C and a lower proportion of tungsten (W) in the materials through which gamma-rays pass, This leads to a decrease in shielding performance and, consequently, an increase in RPLGD response. On the other hand, when gamma-rays enter from positive angles, they come from the side of W, resulting in a higher proportion of W and a lower proportion of C, which increases shielding performances and decreased RPLGD response, Therefore, it can be concluded that the response of the RPLGD to gamma-rays at version irradiation angles is significantly influenced by the shielding performance of the two materials on the outer side of the filter.

3.1.2. *Optimization of filter placement*

To reduce the influence of irradiation angles, it is necessary to design the arrangement such that the same trend is exhibited for both positive and negative angles, while also minimizing the discrepancy compared to 0 deg. Therefore, to mitigate the contributions from oblique incidence from the upper and lower direction, covers were placed above and below the filter, as shown in Fig. 8. In this setup, the order of the filter materials (C, Ni, W) was changed, and three patterns of filter configurations were considered as presented in Fig. 8. In each pattern, the filters and the filter overs were arranged so that gamma-rays could pass the same materials for both positive and negative irradiation angles of gamma-rays. The simulation results are shown in Fig. 9.

By using the filter covers, it was possible to reduce the error for irradiation angles up to ±30 deg. However, for angles of 45 and 60 deg, the three filters exhibited significantly different errors. Examining the values in Fig. 9 with absolute values, the CNiW filter was very close in error to the case without a cover among three filters. This indicates that the arrangement order of the filter materials is also important for reducing the influence of irradiation angles. Additionally, at −45 and −60 deg, the errors increased, inducing excessive shielding. This is likely

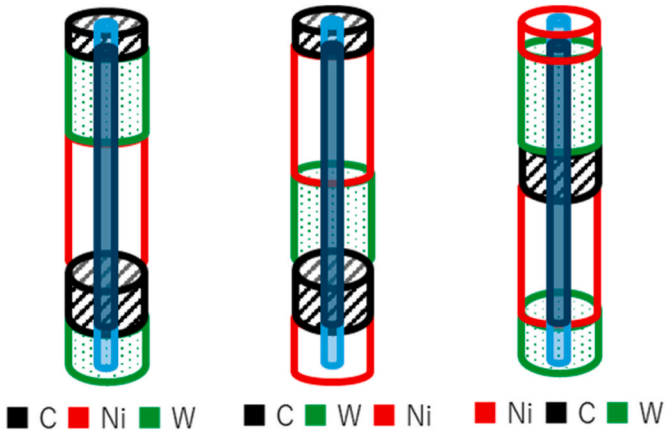

Fig. 8. Schematic diagram showing different setups with three filters and filter covers in both ends.

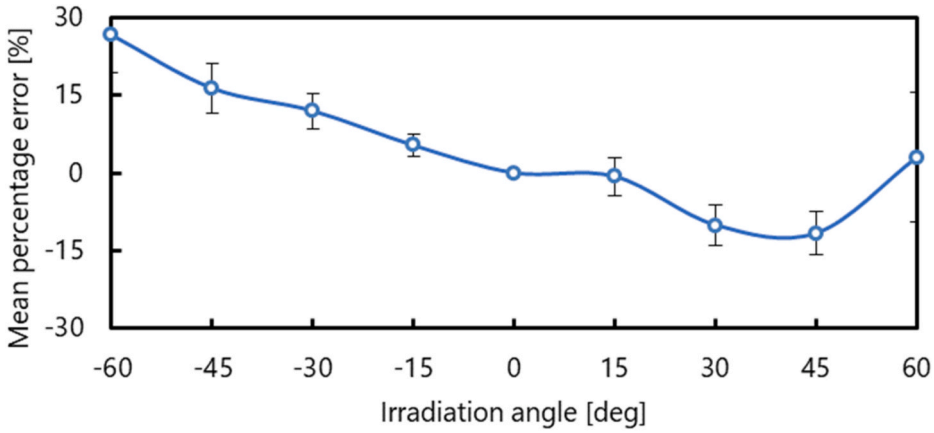

Fig. 7. Error relative to 0 deg for each irradiation angle.

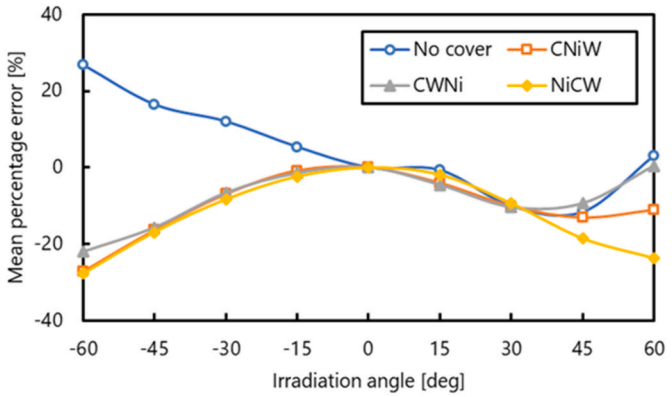

Fig. 9. Average percentage errors for each irradiation angle when using the filter covers in Fig. 12.

due to the placement of W, which affects shielding performances of gamma-rays of all energies. Therefore, it is considered that high atomic number materials should not be used for the filter cover materials.

As mentioned in section 3.1.1, the response of the RPLGD is significantly influenced by the performance of the materials on the outer side of the filter. Furthermore, using high atomic number materials for the filter cover results in larger errors. Taking these factors into account, the order of materials was changed so that the atomic number decreases from the center of the filter towards the outside, as shown in Fig. 10.

3.1.3. *Materials selection for the filter cover*

Based on the filter in Fig. 10, the filter cover materials were chosen for their ease of manufacturing and availability. Specifically, C and Ni, which are used in the current filter, were selected, along with Al and Ti, which have atomic numbers between and farther apart from C and Ni and are also solid materials. PHITS simulations were conducted for angles ranging from −60 deg to 60 deg. The simulation results are shown in Fig. 11. The irradiation distance and gamma-ray energy are the same as the conditions shown in Section 2.3. The results are presented as average percent errors relative to the 0 deg angle.

From the results, when carbon (C) was used for the filter cover, the error was approximately 10 % compared to 0° only at angles of ±60 deg,

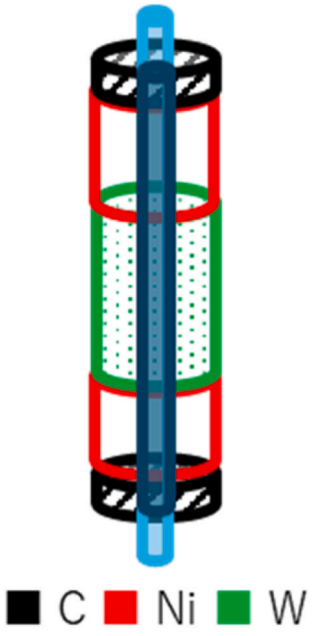

Fig. 10. Optimized filter placement.

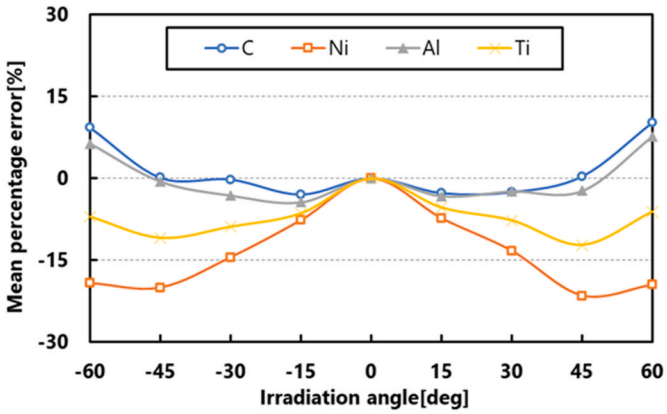

Fig. 11. Error relative to 0 deg for each irradiation angle with each filter cover.

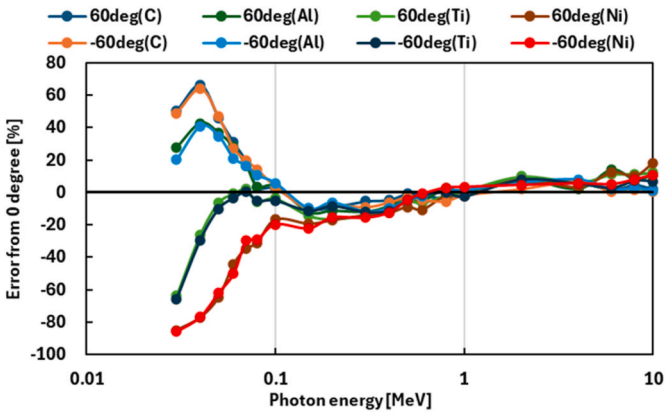

Fig. 12. Errors at ±60 deg irradiation relative to 0 deg for each energy with C, Al, Ti and Ni filter cover.

while at other angles the error remained within about 3 %, showing good angular dependency. When nickel (Ni) or titanium (Ti) was used for the filter cover, the error increased significantly on the negative side across all irradiation angles. On the other hand, when aluminum (Al) was used, the error was within 5 % for angles up to ±45 deg and even at ±60 deg the maximum error was 8 %, indicating an improvement in angular dependency compared to C. However, the vertical axis of Fig. 11 shows the average error over all energy ranges, meaning that large errors at high or low energies may have canceled each other out. Therefore, Fig. 12 shows the errors for each energy range from 0.03 to 10 MeV when the filter cover was made of C, Al, Ti and Ni at irradiation angles of ±60 deg, compared to 0 deg. The irradiation distance and gamma-ray energy are the same as the conditions shown in Section 2.3. From Fig. 12, it can be seen that at all angles, errors increased in the low-energy range of 0.03–0.06 MeV. With the C filter cover, the maximum error was 66 % at 60 deg and 63 % at −60 deg, while the error improved when using an Al filter cover, it still reached maximum of 43 % at 60 deg and 41 % at −60 deg, meaning that angular dependency was not sufficiently improved. Additionally, data for Ti and Ni are included in Fig. 12 for comparison, however, both show large negative errors at low energy range of 0.03–0.06 MeV. Especially, when using the Ni filter cover, the error in the negative direction becomes significantly large, reaching up to 85 %. These are likely due to the atomic numbers of Ti and Ni, which are thought to have significantly shielded low-energy gamma-rays. From Fig. 12, it can be seen that Al has a large positive error at low energy. While Ti shows a large negative error. Based on these observations, we considered using a material with a higher atomic number than Al but lower than Ti, which is also solid. Considering the choice of properties between Al and Ti, we adopted a Ti–Al alloy. Alloys allow for the

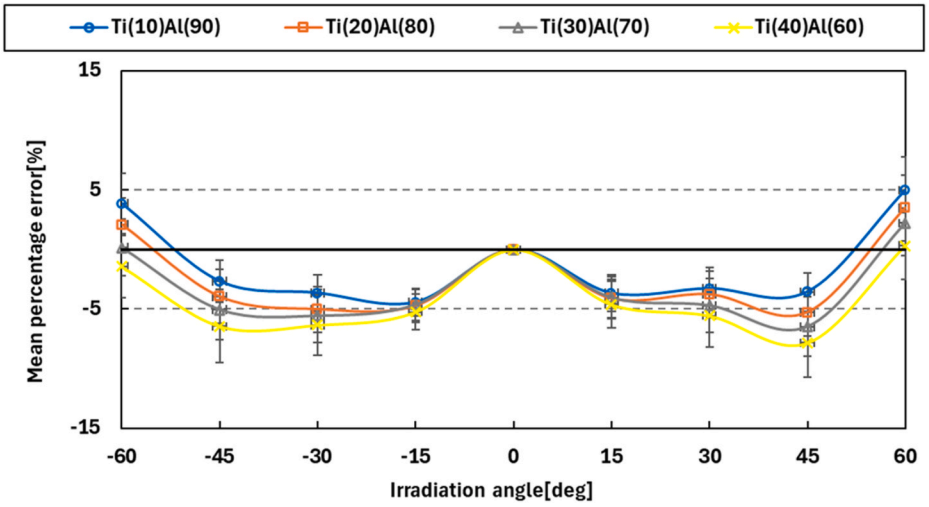

Fig. 13. Error from the 0 deg for each filter cover.

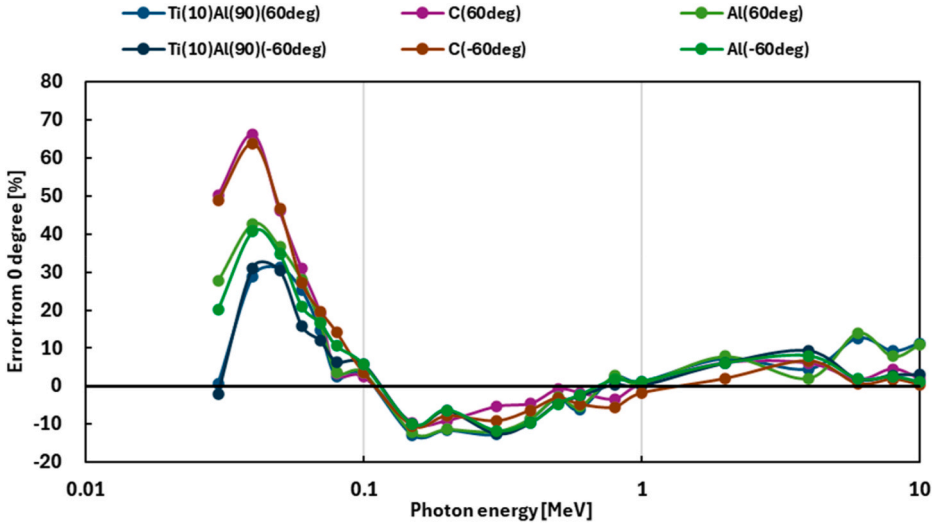

Fig. 14. Errors at ±60 deg irradiation relative to 0 deg for each energy with Ti(10)Al(90) filter cover.

adjustment of effective atomic number and density by modifying the composition, making them suitable as filter cover materials. To determine the optimal composition ratio, we used four validations of the filter cover, Ti(10)Al(90), Ti(20)Al(80), Ti(30)Al(70), Ti(40)Al(60). Irradiation simulations were conducted using PHITS at angles between −60 deg and 60 deg, with a source distance if 5 cm. A monoenergetic point gamma-ray source was employed, and energies selected from 0.03 to 10 MeV, as listed in Table 1. The simulation results are shown in Fig. 13. The reason for using a higher ratio of Al compared to Ti is that showed better angular dependency.

From Fig. 13, it was found that Ti(10)Al(90) showed good results with an error within 5 % for all irradiation angles. Fig. 14 shows the error between 0 deg and ±60 deg irradiation for each energy when using a filter cover made of Ti(10)Al(90). From Fig. 14, even in the low-energy range of 0.03–0.06 MeV, the error was smaller compared to C and Al, with a maximum error of about −24 % at 60 deg and about −30 % at −60 deg, indicating an improvement in angular dependence at low energies. Fig. 15 shows a comparison of the filter response and the air kerma coefficient when using a filter cover of Ti(10)Al(90). Additionally, as a performance evaluation index for the filter, the MAPE (Mean Percentage Error) was calculated using equation (15), which showed 6.1 %, indicating that a filter capable of reproducing the air kerma coefficient with an error within 10 % was successfully designed.

4. Experimental conditions

Filters designed based on PHITS simulations were actually produced, and irradiation experiments were conducted. The irradiation experiments used the gamma-ray standard source shown in Section 4.1, and the experimental setup is described in Section 4.2.

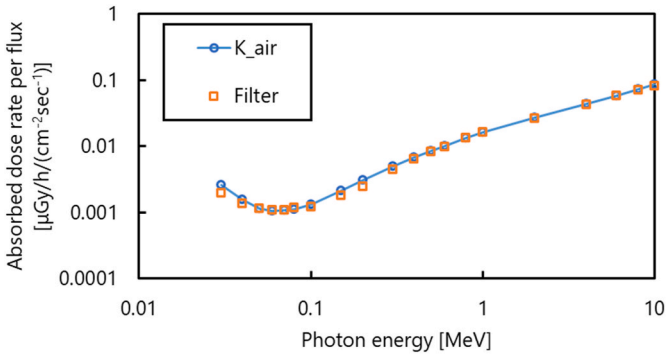

Fig. 15. Comparison result between the filter response and air kerma coefficient when the filter cover is compared of Ti(10)Al(90).

Table 3
Characteristics of the gamma-ray sources [24].

Nuclide	Intensity[a] [MBq]	Half life [year]	Gamma-ray energy [MeV]	Emission ratio [%]
^{133}Ba	0.852	10.52	0.0532	2.2
			0.0796	2.6
			0.081	34.1
			0.276	7.2
			0.303	18.3
			0.356	62.1
			0.384	8.9
^{137}Cs	1	30.17	0.661	85.1
^{60}Co	1.06	5.27	1.173	99.9
			1.333	100

[a] At Feb. 21, 2013.

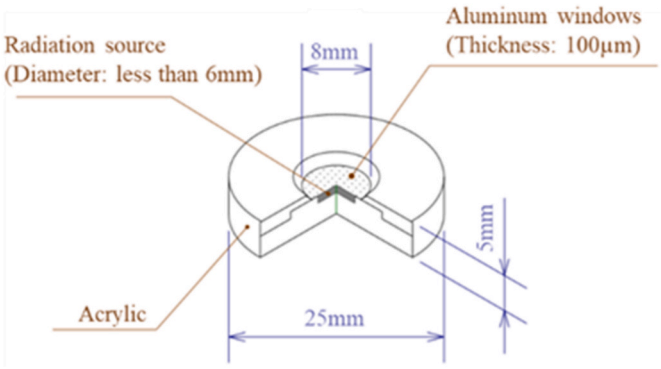

Fig. 16. The gamma-ray standard source of 402 type [25].

4.1. Standard gamma-ray sources

In this study, the monoenergetic gamma-ray standard sources of ^{133}Ba, ^{137}Cs and ^{60}Co were used. The characteristics of the gamma-ray sources are summarized in Table 3 [24]. The standard sources used in this experiment are point sources with a diameter of less than 6 mm, and the external appearance of the standard sources is depicted in Fig. 16.

4.2. Experimental setup

Fig. 17 shows (a) schematic diagram of the experimental setup at 0 deg. and (b) photo of the experiment. The area outside the reading region of the RPLGD is covered with a filter cover. The distance from the source to the center of the RPLGD is the same as the calculation conditions for the response function matrix. Three dosimeters were placed on a polystyrene base, and irradiation was carried out for 2–3 days. Fig. 18 illustrates, similar to Fig. 17, the experimental setup at angles of 15 deg and 30 deg. As shown in the figure, the position of the source was raised using polystyrene to change incident angles of gamma-rays. The polystyrene heights of 2.5 cm and 5.0 cm were used. Also, the distances from the source to the RPLGDs are different from the 0 deg irradiation case in Fig. 17. In summary, the positions of the RPLGDs were adjusted by the height of the source and the distance to the source to achieve the desired irradiation angles. Fig. 19 provides a schematic diagram illustrating how to determine the height of the source and the position of the dosimeter. The source height, dosimeter position, and irradiation distance necessary to achieve the desired irradiation angle are shown in Table 4. In this study, irradiation experiments at 45 deg and 60 deg were also conducted. However, as shown in Table 4, the experimental setup differs only in the height of the source and the distance to the RPLGD and is largely the same as that shown in Fig. 18.

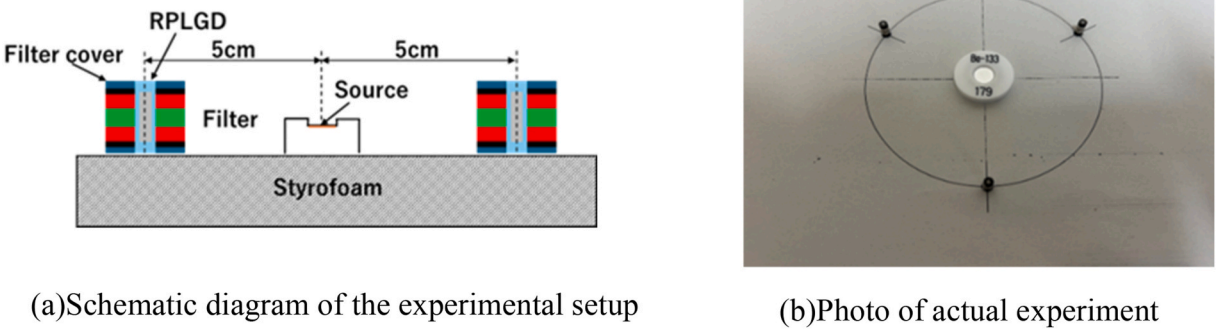

Fig. 17. The irradiation experimental setup at a 0 deg irradiation angle.

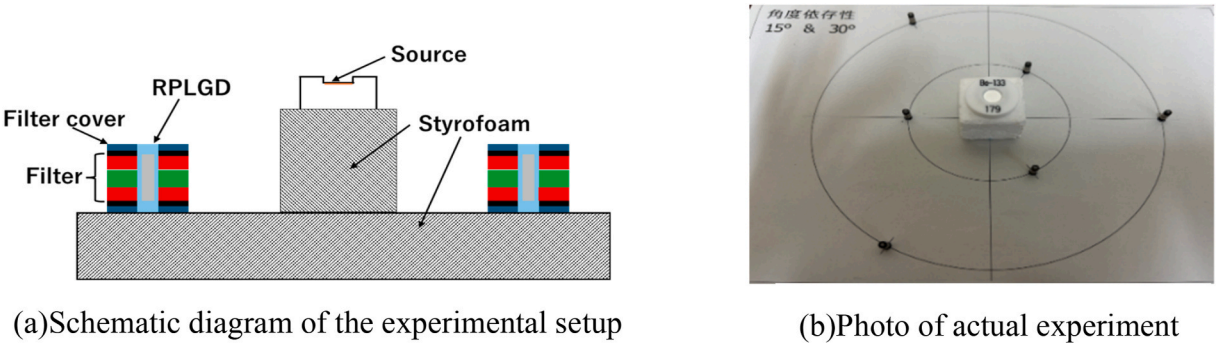

Fig. 18. The irradiation experimental setup at angles of 15 deg and 30 deg.

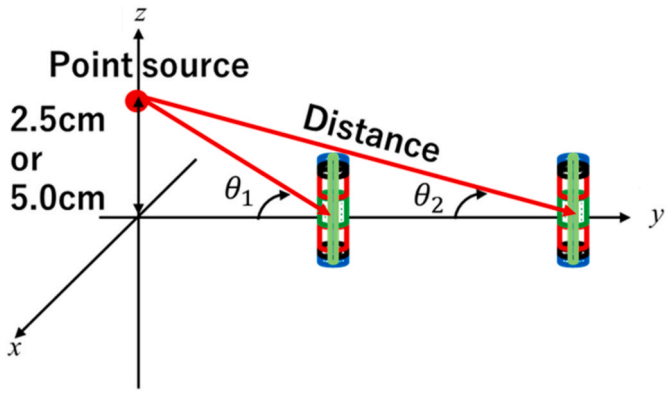

Fig. 19. Method for determining the source height and dosimeter position.

Table 4
Source height, dosimeter position, and irradiation distance for each angle.

Angle [deg]	Height of source [cm]	Position of RPLGD [cm]	Irradiation distance [cm]
0	0	5.0	5.0
15	2.5	9.3	9.7
30	2.5	4.3	5.0
45	5.0	5.0	7.1
60	5.0	2.9	5.8

5. Irradiation experiments with standard gamma-ray sources

The Ti(10)Al(90), which showed the best performance in Section 3.1.3, is difficult to obtain commercially and is therefore not suitable for fabricating filter covers for irradiation experiments. Therefore, we fabricated a filter cover using Ti(30)Al(70) (a commercially available product) instead, which exhibited similarly good performance to other combinations of Ti and Al. Irradiation experiments were conducted using the experimental setup shown in Fig. 17 and standard gamma-ray sources (^{133}Ba, ^{137}Cs, ^{60}Co). Fig. 20 shows an overview of the fabricated filter. Fig. 21 compares the filter response and the air kerma coefficient when using filter covers of Ti(30)Al(70) and Fig. 22 shows a comparison of the experimental values, the simulation results with PHITS and the theoretical values derived from the air kerma coefficient.

From Fig. 22, it can be confirmed that for all radiation sources, the experimental errors are below 10 %, and the PHITS calculation values and the theoretical values are in agreement within experimental error range.

Next, to verify angular dependence, irradiation experiments were conducted using the experimental setup shown in Fig. 18. Fig. 23 shows a comparison between the experimental values and the simulation

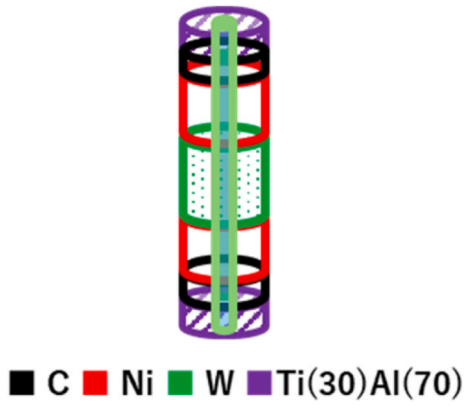

Fig. 20. Designed filter with Ti(30)Al(70) filter cover.

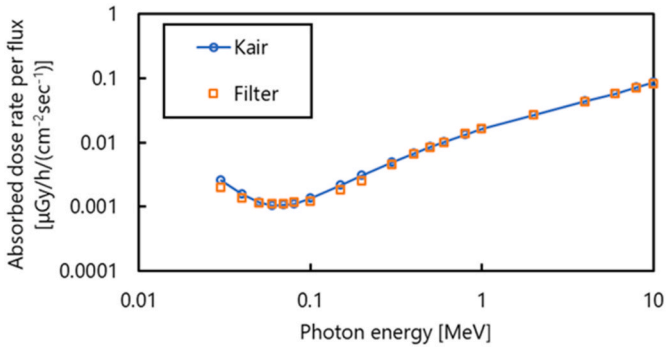

Fig. 21. Comparison results between the filter response and air kerma coefficient when the filter cover is composed of Ti(30)Al(70).

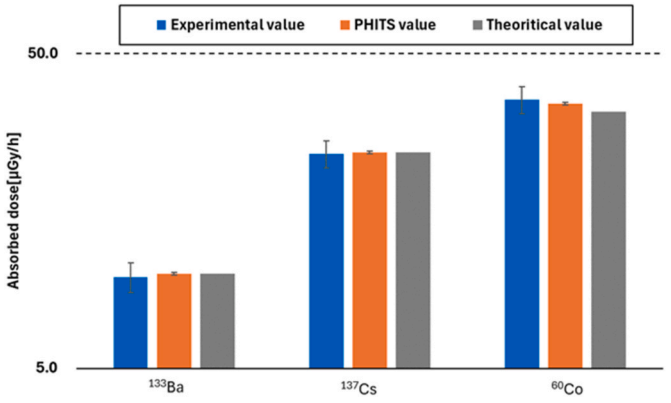

Fig. 22. Comparison of absorbed dose measurement results using standard gamma-ray sources, ^{133}Ba, ^{137}Cs, ^{60}Co with PHITS simulation results and theoretical value.

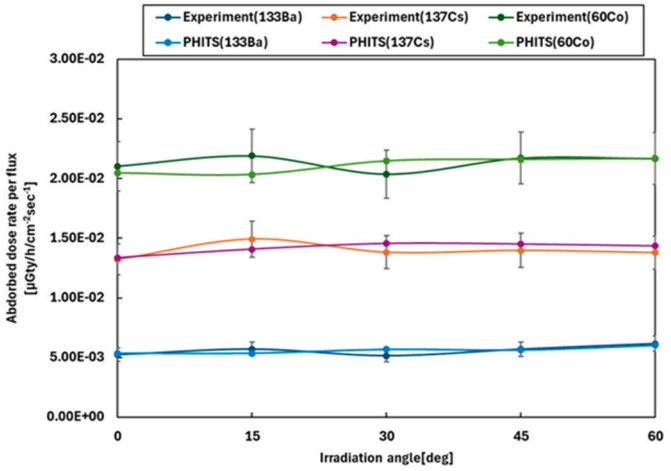

Fig. 23. Comparison of absorbed dose measurement results using standard gamma-ray sources, ^{133}Ba, ^{137}Cs, ^{60}Co with PHITS simulation results at irradiation angles of 15–60°..

results from PHITS, and Fig. 24 presents the derivation from 0 deg irradiation for each standard source when using the Ti(30)Al(70) filter cover.

From Fig. 23, it can be confirmed that for all radiation sources, the experimental errors are below 10 %, and the PHITS calculation values are in agreement within the experimental error range. Next, regarding the deviation from 0 deg, Fig. 24 shows that for all sources, the deviation

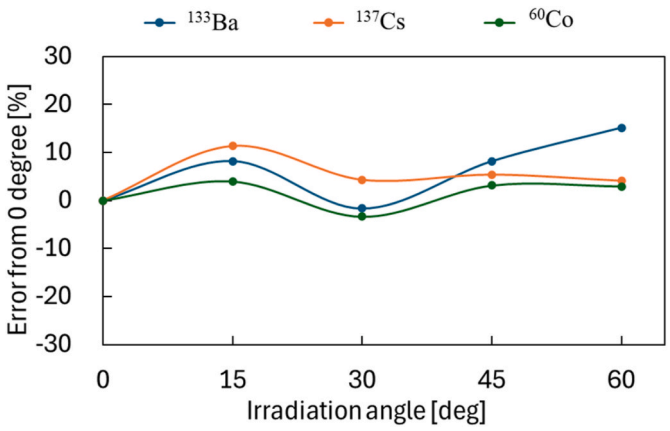

Fig. 24. The error from the 0 deg irradiation for each standard gamma-ray source of Ti(30)Al(70).

from 0 deg was within 20 %, and particularly for the irradiation experiments using ^{60}Co, which emits gamma rays above 1 MeV, the deviation was within 5 % at all irradiation angles.

6. Conclusion

In this study, we proposed and examined the shielding material filter method for gamma-ray fields. Previous filter designs had shown significant errors when gamma-rays entered the RPLGD at large irradiation angles, indicating a need for improvement in angular dependence. To improve angular dependence, this study implemented thinning of filters, optimizing of their arrangement, and adoption of filter covers. Through analysis with PHITS and filter design using Bayesian estimation, as well as irradiation experiments using gamma-ray standard sources, the following conclusions were drawn.

1 By optimizing the thinning of the filter and its arrangement, and by adopting a Ti–Al alloy (Ti(10)Al(90)) for the filter cover material, it was found that the average percentage error could be kept within 5 % when the irradiation angle was within ±60 deg
2 Irradiation experiments were conducted using gamma-ray standard sources (^{133}Ba, ^{137}Cs, ^{60}Co) at 0 deg for the designed filter. The results showed that the experimental errors were below 10 %, and the PHITS calculation values and the theoretical values are in agreement within the experimental error range.
3 Irradiation experiments using gamma-ray standard sources (^{133}Ba, ^{137}Cs, ^{60}Co) at angles ranging from 15 to 60 deg were conducted on the designed filter cover. For all radiation sources, the experimental errors were below 10 %, and the PHITS calculation values and the theoretical values were in agreement within the experimental error range. Additionally, the ratios of absorbed doses at each angle to the dose at irradiation angle 0 deg for each source indicated agreement within 20 % for all three sources. Notably, in the irradiation experiments using ^{60}Co, which emits gamma-rays above 1 MeV, the results showed consistency within 5 % across all irradiation angles

In this study, a shielding filter method for gamma-rays was developed, designing fabricating and verifying a filter capable of accurately measuring high-energy gamma rays. The practicality of the filter was confirmed through experimental validation. However, we recognize that the filter material designed in this study contains toxic substances, and we consider that the toxicity can be mitigated by encapsulating the entire filter. Moving forward, we plan to design and fabricate a filter capable of accurately controlling the response to neutrons. Ultimately, we aim to produce two types of filters to verify their applicability in mixed neutron and gamma-ray fields.

CRediT authorship contribution statement

K. Aoki: Writing – original draft. **Z. Xu:** Methodology. **M. Matsuki:** Validation. **S. Kusaka:** Data curation. **S. Tamaki:** Writing – review & editing. **F. Sato:** Project administration. **I. Murata:** Supervision, Funding acquisition.

Declaration of competing interest

The authors declare the following financial interests/personal relationships which may be considered as potential competing interests: Isao Murata reports financial support was provided by Japan Society for the Promotion of Science. If there are other authors, they declare that they have no known competing financial interests or personal relationships that could have appeared to influence the work reported in this paper.

Acknowledgements

We are grateful to Dr. Mitsuhiro Matsumoto of Osaka University for his warm help in carrying out the present experiments. We also thank Messrs. Tatsuya Watanabe and Yukihiko Sejimo of Chiyoda Technol Corporation for their disclosing detailed data on the characteristics of RPLGD and the dosimeter readers. This work was supported by JSPS KAKENHI [grant number JP19H02648].

Data availability

Data will be made available on request.

References

[1] Stella Pharma, BNCT (boron neutron capture therapy). https://stella-pharma.co.jp/en/bnct/, 2024, July 1.
[2] W.A.G. Sauerwein, R.L. Moss, European Comission, Joint Research Centre, Institute for EnergyRequirements for boron neutron capture therapy (BNCT) at a nuclear research reactor. https://ec.europa.eu/jrc/en/publication/books/requirements-boron-neutron-capture-therapy-bnct-nuclear-research-reactor.
[3] C. Aschan, M. Toivonen, S. Savolainen, T. Seppälä, I. Auterinen, Epithermalneutron beam dosimetry with thermoluminescence dosemeters for boron neutroncapture therapy, Radiat. Protect. Dosim. 81 (1) (1999) 47–56. https://doi.org/10.1093/oxfordjournals.rpd.a032569.
[4] F.Y. Hsu, M.C. Chiu, Y.L. Chang, C.C. Yu, H.M. Liu, Estimation of photon and neutron dose distributions in the THOR BNCT treatment room using dual TLD method, Radiat. Meas. 43 (2–6) (2008) 1089–1094. https://doi.org/10.1016/j.radmeas.2007.10.014.
[5] D. Moro, P. Colautti, M. Lollo, J. Esposito, V. Contre, L. De Nardo, A. Ferretti, C. Ceballos, BNCT dosimetry performed with a mini twin tissue-eqivalent proportional conters (TEPC), Appl. Radiat. Isot. 67 (7–8) (2009) 171–174. https://doi.org/10.1016/j.apradiso.2009.03.042.
[6] IAEA, Current Status of neutron capture therapy, IAEA 2001 (8) (2001) 75–77.
[7] M. Marrale, T. Schmitz, S. Gallo, G. Hampel, A. Longo, S. Panzeca, L. Tranchina, Comparison of EPR response of alanine and GD_2O_3-alanine dosimeters exposed to TRIGA Maitz reactor, Appl. Radiat. Isot. 106 (2015) 116–120. https://doi.org/10.1016/j.apradiso.2015.08.016.
[8] G. Alejandro, J. Longhino, R.N. Alvarez, E. Pawlak, A dual natural lithium formate/L-alanine EPR dosimeter for a mixed radiation field in a boron neutron capture therapy irradiation facility, J. Phys. Appl. Phys . 53 (2020) 165001. https://doi.org/10.1088/1361-6463/ab6e45.
[9] G. Gambarini, E. Artuso, D. Giove, M. Felisi, L. Volpe, L. Barcaglioni, S. Agosteo, L. Garlati, A. Pola, V. Klupak, L. Viererbl, M. Vins, M. Marek, Study of suitability of Fricke -gel -layer dosimeters for in-air measurements to characterize epithermal/thermal neutron beams for NCT, Appl. Radiat. 106 (2015) 145150. https://doi.org/10.1016/j.apradiso.2015.07.036.
[10] H. Horiike, I. Murata, T. Iida, S. Yoshihashi, E. Hoashi, I. Kato, N. Hashimoto, S. Kuri, S. Oshiro, Liquid Li based neutron source for BNCT and science application, Appl. Radiat. Isot. 106 (2015) 92–94. https://doi.org/10.1016/j.apradiso.2015.07.026.
[11] Enhancing the effectiveness of boron neutron capture therapy (BNCT) for cancer treatment, Impact 2021 (8) (2021) 19–21. https://doi.org/10.21820/23987073.2021.8.19.
[12] I. Murata, S. Kusaka, K. Minami, N. Saraue, S. Tamaki, I. Kato, F. Sato, Design of SPECT for BNCT to measure local boron dose with GAGG scintillator, Appl . Radiat 181 (2022) 10056. https://doi.org/10.1016/j.apradiso.2021.110056.
[13] R. Yokota, H. Imagawa, Radiophotoluminescent centers in silver-activated phosphate glass, Physical Society of Japan 23 (5) (1966) 1038–1048.

[14] K. Hiramatsu, S. Yoshihashi, S. Kusaka, F. Sato, E. Hoashi, I. Murata, Gamma -ray dose measurement with radio-photoluminescence glass dosimeter in mixed radiatio field for BNCT, EPJ Web Conf 15 (3) (2017) 1–9. https://doi.org/10.1051/epjconf/201715304009.
[15] K. Tochitani, K. Tomiyoshi, T. Inoue, F. Kamisaki, M. Matsuki, K. Hiramatsu, K. Aoki, S. Kusaka, S. Tamaki, F. Sato, I. Murata, Control of RPLGD for gamma-ray dose measurement using lead filters for BNCT, Appl. Radiat. Isot. 199 (2023) 110897. https://doi.org/10.1016/j.apradiso.2023.110897F.
[16] F. Kamisaki, T. Inoue, K. Tomiyoshi, M. Matsuki, K. Aoki, S. Kusaka, S. Tamaki, F. Sato, I. Murata, Accurate gamma-ray dose measurement up to 10MeV by glass dosimeter with a sensitivity control filter for BNCT, Appl. Radiat. Isot. 209 (2024) 111299. https://doi.org/10.1016/j.apradiso.2024.111299.
[17] Asahi Techno Glass Corporation. Explanation material of RPL glass dosimeter: small element System, Tokyo, Japan, 2013.
[18] F. Araki, T. Ikegami, T. Ishidoya, H.D. Kubo, Measurement of Gamma-Knife helmet output factors using a radiophotoluminescent glass rod dosimeter and a diode detector, Med. Phys. 30 (8) (2003) 1976–1981. https://doi.org/10.1118/1.1587451.
[19] Spectra-Physics, Explorer One^{TM} compact UV and green lasers, 2023, September. https://www.spectra-physics.com/en/f/explorer-one-compact-laser.
[20] ICRP, Conversion coefficients for use in radiological protection against external radiation, ICRP Publication 74. Ann. ICRP 26 (1996) 3–4. https://doi.org/10.1016/0146-6453(81)90127-5.
[21] S. Iwasaki. A New Approach for Unfolding PHA Problems Based Only on Bayes's Theorem, Proceeding of the 9th International Symposium on Reactor Dosimetry, Prague(Czech Republic), 1996, pp. 245–252.
[22] Y. Nauchi, S. Iwasaki, Convergence of unfolded spectrum with response function for single radiation based on Bayes' theorem, Nucl. Instrum. Methods Phys. Res. Sect. A Accel. Spectrom. Detect. Assoc. Equip. 735 (2014) 437–443. https://doi.org/10.1016/j.nima.2013.09.064.
[23] T. Sato, Y. Iwamoto, S. Hashimoto, T. Ogawa, T. Furuta, Abe, T. Kai, P.E. Tsai, N. Matsuda, H. Iwase, N. Shigyo, L. Sihver, K. Niita, Features of particle and Heavy Ion transport code system (PHITS) version 3.02, J. Nucl. Sci. Technol. 55 (6) (2018) 684–690. https://doi.org/10.1080/00223131.2017.1419890.
[24] ICRP, Nuclear decay data for dosimetric calculations, ICRP Publication 107, Ann. ICRP 38 (3) (2008).
[25] Japan Radioisotope Association. https://www.jrias.or.jp/products/pdf/RI-catalog-03-20230401.pdf. RO-catalog-03-20230401.pdf.